Self-Organization, Structure, Dynamic Properties, and Surface Morphology of Silica/Epoxy Films As Seen by Solid-State NMR, SAXS, and AFM

Jiri Brus,* Milena Špírková, Drahomíra Hlavatá, and Adam Strachota

Institute of Macromolecular Chemistry, Academy of Sciences of the Czech Republic, Heyrovsky sq. 2, 162 06 Prague 6, Czech Republic

Received October 25, 2003; Revised Manuscript Received December 2, 2003

ABSTRACT: The high degree of self-assembling of epoxide-based products made from functionalized organosilica building blocks, functionalized oligo(oxypropylene)-diamine and/or -triamine, and colloidal silica nanoparticles was evidenced by solid-state NMR spectroscopy, small-angle X-ray scattering (SAXS), and atomic force microscopy (AFM). Under optimized conditions of preparation, isolated siloxane cagelike clusters arise in the reaction mixture. No cleavage of oxirane rings occurs before thermal curing, and thus the whole process is well controlled. The presence of silica nanoparticles accelerates the kinetics of polycondensation and affects the condensation rate of siloxane units in final products. Two-dimensional solid-state NMR experiments (2D CRAMPS, 2D $^{1}H-^{13}C$ and $^{1}H-^{29}Si$ HETCOR, WISE) revealed differences in structure and segmental dynamics of final films as well as in self-organization and homogeneity degree depending on reaction conditions. Ideally, siloxane cagelike clusters are regularly dispersed within the bulk and oxypropylene chains form phase which separates organic tails of siloxane clusters. The SAXS determined distance between clusters (1.8 nm) well corresponds to the constraints determined by NMR spin-diffusion experiments. Polymer interaction with silica nanoparticles is confirmed by two-dimensional $^{1}H-^{29}Si$ HETCOR experiments.

Introduction

New nanocomposite materials can be formed if controlled heterogeneity of the structure on the nanometer scale is possible. As the molecular-scale morphology plays an important role in achieving macroscopic properties of molecular and supramolecular assemblies, the synthetic goal is to prepare multiphase micro- or nanoheterogeneous systems with desired and tunable properties. To achieve this goal, a detailed multidisciplinary characterization is necessary: the correlations between the composition, mechanical, viscoelastic, optical, and other macroscopic properties are essential information. In addition, surface morphology characteristics and determination of surface properties are unavoidable specifications for coating applications.[1−4]

Organic−inorganic hybrid polymers with an in situ created inorganic phase are typical examples of nanocomposite materials, which have received significant interest in the past few years. The modification of organic matrix with siloxane domains formed by sol−gel process of alkoxysilanes is one of the ways of their preparation. The resulting structures depend on the reaction conditions and vary from monodisperse silica particles to polymer networks.[5] In current polymer science much interest is focused on the controlled design of ordered superstructures based on the self-assembly of carefully chosen building blocks. A combination of appropriate processing conditions with adequate organic and inorganic components dictates the morphology, molecular structure, and features of hybrid materials. Thus, a suitable choice of functionalized siloxane monomers and reaction conditions leads to the formation of nanoheterogeneous networks with well-organized cagelike structures or cycles, up to nearly homogeneous bicontinuous systems. The recently described spontaneous formation of polyhedral oligomeric silsesquioxane[6] (POSS) units from functionalized trialkoxysilanes may lead to the formation of star polymer systems with well-defined architecture.

Building units suitable for preparation of hybrid networks are functionalized alkoxysilanes, poly(oxypropylene) end-capped with primary amino groups, and colloidal silica nanoparticles. Addition of nanoparticles of various composition, size, and shape into the organic polymerizable system increases variability of nanocomposite preparation[7] and resulting behavior. Possessing available functional groups for the formation of covalent and noncovalent bonding, they interact with the polymer matrix, leading to intercalation of polymers and formation of new partially ordered structures. While trialkoxysilanes are widely used monomers,[8−12] the use of functionalized dialkoxy(alkyl)silane analogues is not widespread although various resulting structures can be expected. Dialkyloxy(alkyl)silanes are prone to cyclization,[13,14] thereby enabling the formation of functionalized cyclics that may self-organize. Recently, we have prepared and characterized a wide range of hybrid films made from [3-(glycidyloxy)propyl]trimethoxysilane (GTMS), diethoxy[3-(glycidyloxy)propyl]methylsilane (GMDES), poly(oxypropylene) of various molecular weights (Jeffamine D-230, D-400, and T-403), and in some cases colloidal silica (SiO_2) particles.[15,16] We screened the influence of composition, functionality, and reaction conditions on the structure of these hybrid products, since the well-tuned properties enable their use as coatings with various kinds of protection.[11,17−19] The variability of final properties was previously demonstrated by static and dynamic mechanical analysis. In this contribution, a high degree of self-organization and regularity of these nanostructured networks based on an epoxy thermosetting matrix and in situ formed

* To whom correspondence should be addressed: tel +420 296 809 380; Fax +420 296 809 410; e-mail brus@imc.cas.cz.

10.1021/ma035608h CCC: $27.50
Published on Web 01/16/2004

Scheme 1. MM+ Optimized Molecular Structure of All Basic Building Blocks[a]

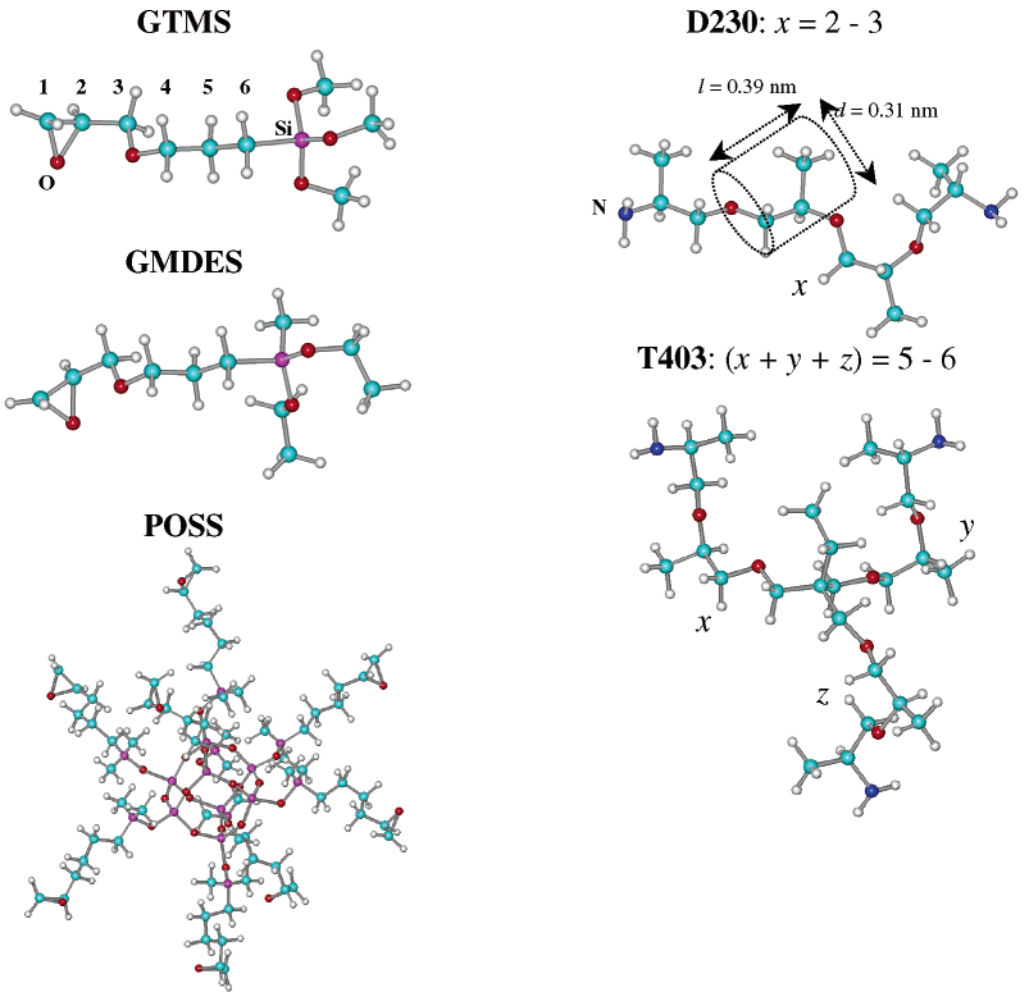

[a] *x*, *y*, and *z* correspond to the number of oxypropylene monomer units within each polymer chain. Average size oxypropylene monomer unit is introduced for Jeffamine D230.

inorganic cagelike structures is demonstrated. A comparison with networks prepared from regular functionalized POSS building blocks is made, and the influence of colloidal silica nanoparticles on the network structure buildup is demonstrated.

If the mechanisms governing the partial ordering and self-assembly are to be better understood, determination of the structure and dynamic behavior of these partially ordered systems is essential. Solid-state NMR spectroscopy is an excellent method providing information on the microstructure, mobility, and conformation of molecules as well as on the composition of these complex and interesting systems without requirement of long-range ordering. Multinuclear solid-state NMR has been used recently to study nanostructure and dynamics of various polymer−nanoparticle composites.[20−24] With the recent development of techniques for detecting proton−proton proximities,[25] solid-state NMR techniques provide important tools to characterize local geometry.

In our study we used ^{13}C and ^{29}Si MAS and CP/MAS NMR spectroscopy to follow structure evolution and to evaluate reaction conditions affecting the final structure and chemical composition of resulting networks. Variable temperature relaxation experiments as well as ^{13}C WISE probed segmental dynamics and homogeneity. Various 2D homonuclear and heteronuclear solid-state correlation experiments employing spin diffusion confirmed the spectral assignment, detected through-space contacts and thus elucidated global architecture and the extent of self-organization at nanometer scale. Established diffraction techniques are complementary to solid-state NMR and offer other type of information about the order of polymer materials. SAXS was hence used to detect long-range periods (diffraction correlation length). The surface morphology and other surface characteristics were investigated by AFM.

Experimental Section

Materials. [3-(Glycidyloxy)propyl]trimethoxysilane (GTMS, Fluka), diethoxy[3-(glycidyloxy)propyl]ethylsilane (GMDES, Fluka), Jeffamine D-230 and T-403 (D230 and T403, Huntsman Corp.), colloidal silica (40% solution in water; $d_{ave} = 29$ nm; Ludox AS-40, Aldrich), and propan-2-ol (Lachema, Czech Republic) were used as received. The POSS octaepoxide was synthesized from the commercial POSS octasilane "$Q_8M_8H_8$" (1,3,5,7,9,11,13,15-octakis(dimethylsilyloxy)pentacyclo]octasiloxane) (Aldrich) and from 5,6-epoxy-1-hexene (Aldrich) via hydrosilylation (excess epoxyhexene, 2% Carstedt catalyst in xylene (Aldrich), 4.45 ppb Pt relative to Si−H; the excess epoxyhexene was removed at vacuum and room temperature). The formulas of all building blocks are given in Scheme 1.

Technique of Preparation of Coating Films. GTMS and GMDES were mixed with water, propan-2-ol, and (in some cases) with colloidal silica particles and stirred at ambient temperature for 24 h ("acid" step). Then the proper amine was added, and the reaction mixture was stirred at ambient temperature for up to 3 h ("alkaline" step) and subsequently

Table 1. Chemical Composition of Resulting Networks, Basic Mechanical and Surface Properties, and Glass Transition Temperature (T_g)

	SiO_2:GTMS:D230 (wt %)	stress at break (MPa)	strain at break (%)	Young modulus (MPa)	toughness[a] (kJ/m^2)	T_g[b] (°C)	F_n[c] (nN)	S_r[c] (GN/m^2)
GTMS	0:73.3:26.7	13.0	6.0	221	8.2	17	298	5.3
GTMS silica	19.8:58.7:21.5	26.2	9.2	660	37.4	20	329	8.8
GMDES	0:75.5[d]:24.5[e]	7.3	31.2	31	30.7	17	322	8.7
GMDES silica	20.5:60.7[d]:18.8[e]	10.7	23.7	54	41.6	23	311	11.3

[a] The energy per unit cross section necessary to break the sample. [b] Determined from dynamic mechanical analysis as the maxima of loss factor. [c] Scratch resistance, S_r; normal force, F_n. [d] GMDES. [e] T403.

poured onto glass or modified-polypropylene (PP) sheets with a ruler of constant thickness and immediately placed into an oven and kept at 80 °C (2 h) and at 105 °C (1 h), (thermal curing). For this study we chose two representatives of films having "above-average" toughness, namely systems GTMS−Jeffamine D-230 at the NH/epoxy ratio $r = 1.5$ and GMDES−Jeffamine T-403 at $r = 1.0$—both SiO_2-free and SiO_2-containing analogues. Two samples (identical in composition, $r = 1.5$, but varying in the method of preparation) made from a regular functionalized POSS building block and D230 were prepared. The film made from POSS and D230 in block (POSS-B) was prepared by mixing of both components pouring on PP sheets and keeping at 120 °C for 120 h. The film prepared from 50% solution in propan-2-ol (POSS-S) was put onto PP sheet, kept (closed and in the presence of saturated alcohol vapor) at 75 °C for 2 h, and then the alcohol was removed; the sheet was heated in air at 80 °C for 3 h and finally at 120 °C for 120 h. The composition and selected properties of studied samples are given in Table 1. (For details, see ref 15.)

NMR Spectroscopy. 1D ^{13}C and ^{29}Si MAS and RAMP/CP/MAS NMR and 2D ^1H-X HETCOR spectra were measured using a Bruker Avance 500 spectrometer. The signal assignment was performed using CPPI (cross-polarization−polarization−inversion) experiment[26] with 55 μs of inverse polarization period. A 2D $^1H-^{13}C$ WISE (wide-line separation) experiment[27] was used with 32 increments and 100 kHz spectral width in ^1H dimension at rotation frequency $\omega_r/2\pi = 5$ kHz. A magic-angle spin-lock pulse (0.5 ms) for CP was used to suppress spin-diffusion.[28,29] 2D $^1H-^{13}C$ and $^1H-^{29}Si$ HETCOR experiments[30] were performed with FSLG (frequency switched Lee−Goldburg) decoupling during the t_1 evolution period consisting 64 increments with dwell time 42.6 μs. Rotation frequency was $\omega_r/2\pi = 12$ kHz. In some cases $^1H-^1H$ spin-exchange delay (0.1−5 ms) was inserted after the t_1 evolution period to detect spin-diffusion buildup curves. $B_1(^1H)$ field intensity of FSLG and TPPM (two-pulse phase-modulated) decoupling[31] corresponds to $\omega_1/2\pi = 89.3$ kHz. $T_1(^{13}C)$ and $T_{1\rho}(^{13}C)$ relaxation experiments were performed at two temperatures (296 and 310 K) with $B_1(^{13}C)$ spin-locking field intensity corresponding to $\omega_1/2\pi = 62.5$ kHz. 2D ^1H CRAMPS (combined rotation and multipulse spectroscopy) experiments were performed on a Bruker Avance DSX 200 NMR spectrometer at MAS frequency $\omega_r/2\pi = 2$ kHz. The BR-24 pulse sequence[32] was used, with a 90° pulse length of 1.8 μs and a large and short delay of 3.8 and 1.0 μs, respectively. The ^1H scale was calibrated with external standard−glycine (low-field NH_3 signal at 8.0 ppm and the high field α-H signal at 2.5 ppm). For 2D correlation experiment,[33] a spin diffusion mixing time was varied from 0.01 to 20 ms.

Atomic Force Microscopy (AFM). Measurements were performed under ambient conditions using a commercial atomic force microscope (MultiMode Digital Instruments NanoScope Dimension IIIa). Olympus oxide-sharpened silicon nitride probes OMCL TR-400 (spring constants 0.02 and 0.08 N/m) and OTR-8PS (spring constants 0.16 and 0.68 N/m) for contact mode and Olympus tapping-mode etched silicon probe (OTESPA, spring constant 42 N/m, resonance frequency at 272 kHz) for tapping mode were used.

Small-Angle X-ray Scattering (SAXS). SAXS measurements were performed using an upgraded Kratky camera with a 60 μm entrance slit and 42 cm flight path. Ni-filtered Cu Kα radiation (wavelength $\lambda = 0.154$ nm) was used and registered with a position-sensitive detector[34] (Joint Institute for Nuclear Research, Dubna, Russia) for which the spatial resolution is ca. 0.15 mm. The intensities were taken in the range of the scattering vector $q = (4\pi/\lambda) \sin\theta$ from 0.06 to 10 nm^{-1} (where 2θ is the scattering angle). The measured intensities were corrected for sample thickness and transmission, primary beam flux, and sample−detector distance.

Results and Discussion

Formation of Films: Hydrolysis, Condensation, and Thermal Curing. A fairly wide composition range of reaction mixtures was studied by ^{13}C and ^{29}Si MAS NMR to follow kinetics of the reaction process and formation of initial building units as well as to predict the final structure of resulting materials. During the "acid" step, hydrolysis and formation of short oligomers (up to tetramers) are predominant in systems without colloidal silica. Extensive polycondensation starts during the "alkaline" step; however, the presence of colloidal silica accelerates condensation reactions even at low pH (Figure 1; ^{29}Si MAS NMR spectra) as NH_4^+ ions stabilizing colloidal silica particles promote the condensation reactions.

No cleavage of oxirane rings occurs during the whole process before thermal curing, leaving these functional groups accessible for organic network build-up (Figure 1; ^{13}C MAS NMR spectra). This confirms separation of sol−gel and polyaddition steps and a good control of the whole process under carefully chosen conditions. Depending on the durations of "acid" and "alkaline" steps, various precondensates with different size and condensation degrees are formed. As they significantly affect the final structure, homogeneity and, consequently, mechanical properties of the resulting films, the periods of "acidic" and "alkaline" steps were optimized to obtain materials with targeted behavior.

In principle, mechanical properties of the final products improve with increasing time of the initial polycondensation step; however, for excessive reaction times, the viscosity of the system grows rapidly and the arising microgel particles lead to a considerable loss of desired properties. The optimum polycondensation degree of GTMS units (q_i) before thermal curing is ca. 0.85, indicating a high portion of cyclization and formation of polycyclic clusters while a high extent of their aggregation is still prevented.

This indicates that isolated starlike epoxy-functionalized building blocks are formed before thermal curing. The optimum condensation degree at the end of the sol−gel step of GMDES units is about $q_i = 0.7$. In both cases polycondensation of siloxane units is finished during thermal curing, in which predominantly formation of cycles occurs.

Chemical Structure of Organic−Inorganic Hybrid Networks. Chemical composition of selected composites was evaluated by analysis of ^{29}Si and ^{13}C CP/MAS NMR spectra as shown in Figures 2 and 3. Signal assignment was based on known chemical shifts

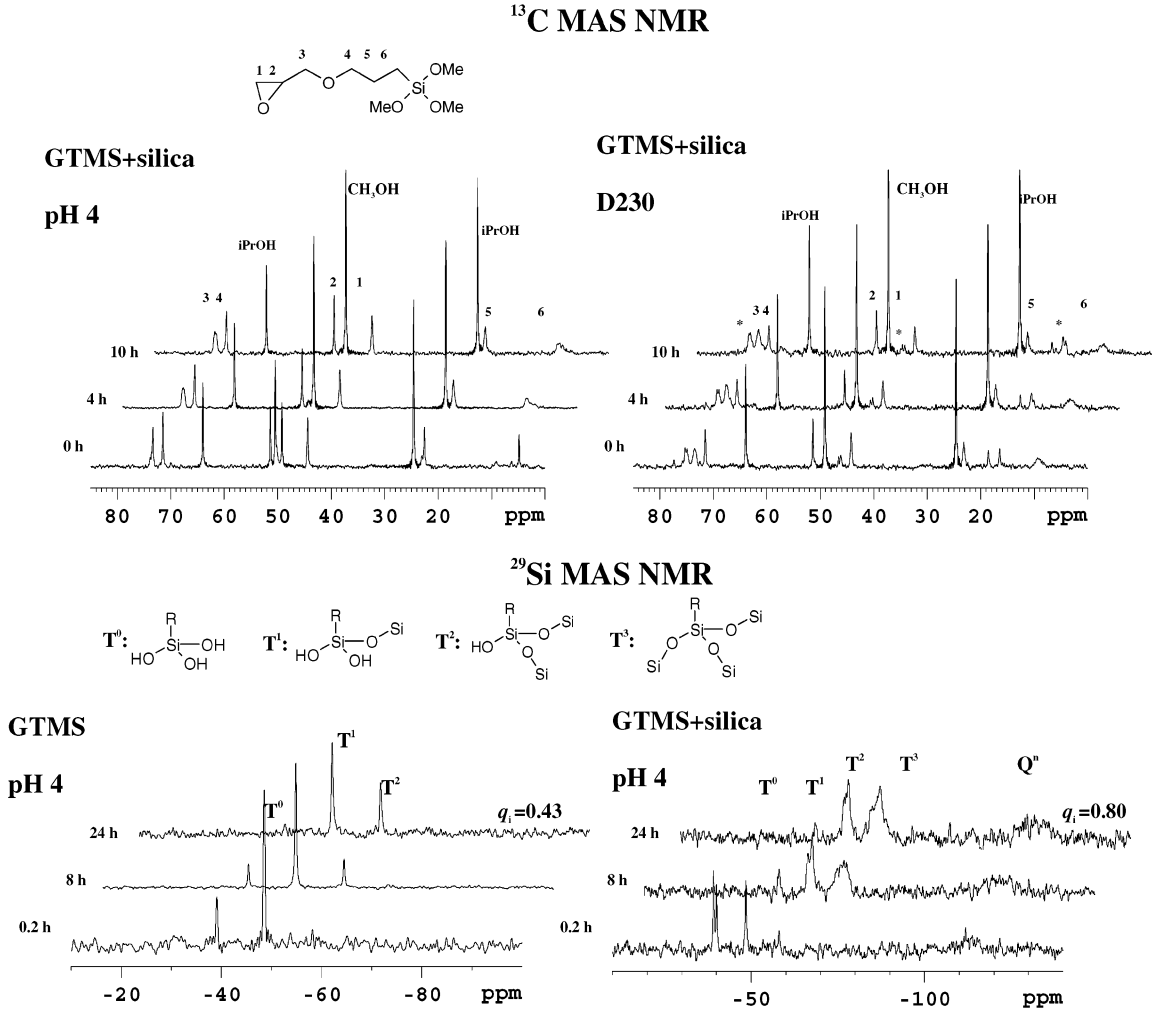

Figure 1. ^{13}C and ^{29}Si MAS NMR spectra of selected reaction mixtures at various reaction times. (Signal assignment of basic structure units and condensation degree q_i of siloxane unit at the end of "acid" step is presented in each spectrum; signals corresponding to oxypropylene unit (CH, CH_2 and CH_3) are marked by asterisks.)

for each monomer, $^1H-^{13}C$ HETCOR and ^{13}C CPPI NMR experiments. As the reactivity of alkylalkoxysilanes decreases with increasing number of alkyl substituents,[35] the final condensation degree q_i of GTMS is therefore much higher than that of GMDES (see Figure 2).

A high amount of T^3 units confirms the formation of highly condensed, compact, and rigid cagelike clusters. The half-width of the ^{29}Si NMR signal of T^3 units (ca. 6 ppm) indicates that the local environment and the geometry around silicon nuclei in the cagelike clusters are not quite random and substantially distorted because the half-width of the corresponding signal of a well-organized POSS network is comparable (ca. 4 ppm). GMDES monomer units form relatively short oligomers (tetramers, pentamers) providing links between oxypropylene chains. As ending monomer units of polysiloxane chains D^1 (nearly 45 mol %) do not increase the network density; their presence results in a significant softening of final coatings. Thus, the ^{29}Si NMR signals of GMDES units are motionally narrowed (ca. 4 ppm for inner monomer units D^2, 5 ppm for D^1). The nonnegligible steric hindrance provided by silica nanoparticles increases the intramolecular condensation rate in the GTMS−silica system and promotes formation of polycyclic siloxane cagelike clusters.

In the GMDES−silica system, which has a lower tendency to condense, the presence of colloidal silica leads predominantly to the formation of large fraction of cycles. This is indicated by a signal at 9.6 ppm corresponding to cyclic trimer (inner monomer units in cycles D_C^2, Figure 2) amounting to almost 5 mol % of siloxane units. This relatively high amount is surprising because the formation of cyclic trimer is energetically disadvantageous compared with the formation of tetramer, the fraction of which is therefore expected to be much higher. Unfortunately, the signal of possible cyclic tetramer cannot be resolved[14] from the signal of linears since their difference is only ca. 2 ppm.

The results show that the epoxy groups are completely consumed during the polyaddition reaction that takes place in alcoholic solution (Figure 3). Only in the case of block polymerization (POSS-B), almost 60 mol % of oxirane rings remain unconsumed. In addition to basic chemical cross-links provided by addition reactions, strongly hydrogen-bonded OH groups affect chemical and physical properties of the networks. In 2D CRAMPS spectra, they were detected with a chemical shift of ca. 5.8 ppm for which an average H···O interatomic distance, r_{HB} of 0.2 nm, was calculated:[36,37]

$$\delta_{iso}\,(\text{ppm}) = \frac{4.65}{r_{HB}\,(\text{nm})} - 17.4 \qquad (1)$$

Segmental Dynamics and Homogeneity: Relaxation Experiments and WISE NMR. An insight into

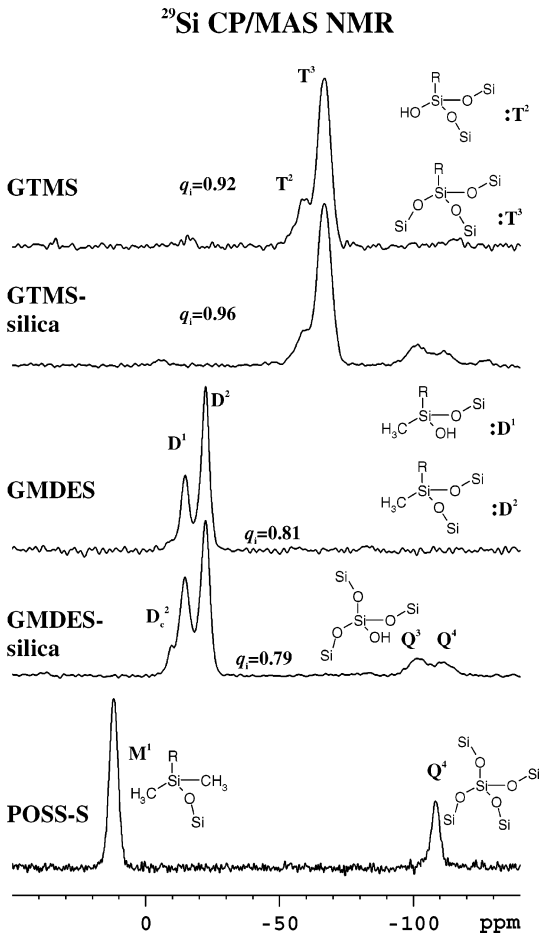

Figure 2. ^{29}Si CP/MAS NMR of selected nanocomposite films. Condensation degree q_i, $q_i = (\sum_{n=1}^{2} nD^n/2) + (\sum_{n=1}^{3} nT^n/3)$ of siloxane units is given in each spectrum. D^n and T^n are the mole fractions of corresponding D^n and T^n structure units. Letters Q, T, D, and M denote theoretical functionality of given structural unit (tetra-, tri-, bi-, and mono-, respectively), and n denotes the actual number of silicon atoms attached to the structure unit by the siloxane bond.

segmental dynamics is provided by NMR relaxation measurements. The T_1(^{13}C) relaxation time is sensitive to high-frequency motions (ca. 125 MHz) while the $T_{1\rho}$-(^{13}C) probes motions in the mid-kilohertz range (ca. 64 kHz). Both types of relaxation measurements were performed at two temperatures (296 and 310 K), thereby enabling an estimation of the activation energy of segmental motion from the Arrhenius relation:

$$\Delta E = R\left(\frac{T_2 T_1}{T_2 - T_1}\right) \ln \frac{R^{13C}_{1(T1)}}{R^{13C}_{1(T2)}} \qquad (2)$$

where $R^{13C}_{1(T2)}$ and $R^{13C}_{1(T1)}$ are ^{13}C relaxation rates determined at temperatures T_2 and T_1.

From the data summarized in Table 2, it is clear that in the GMDES−silica network the estimated activation energies ΔE of high-frequency motions are remarkably lower for CH−N, CH_2−N, and CH_2−Si segments compared with GTMS−silica, which corresponds to larger overall flexibility. In contrast, the low-frequency motions of the CH−N and CH_2−N branching segments are more hindered in GMDES-based networks as a result of a lower number of oxypropylene units in amine moieties (cf. Scheme 1), which ensures mechanical strength of these networks (Table 1). The CH_2−Si units in GMDES-based networks, which are incorporated in short siloxane chains or small cycles, are not immobilized at all. This confirms that these siloxane chains increase elasticity and softening of resulting films. In contrast, the low-frequency motions of these CH_2−Si groups in GTMS-based networks built in to large and compact cagelike clusters are remarkably hindered. The presence of these clusters thus significantly increases the strength of GTMS-based networks. The absence of silica particles releases motion of all segments, and the most pronounced decrease in ΔE was observed for CH_2−Si units in GTMS network. This confirms that a part of these units is coupled to their surface if silica particles are present.

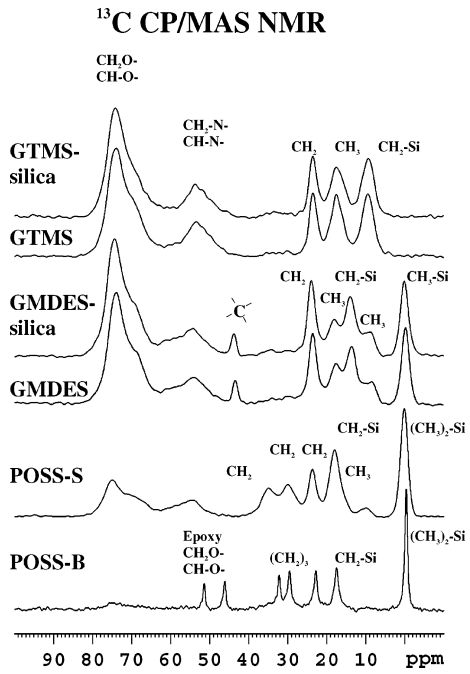

Figure 3. ^{13}C CP/MAS NMR of selected nanocomposite films. Signal assignment based on CPPI and ^{1}H−^{13}C HETCOR experiments is given.

Variability in segmental mobility of the GMDES−silica system is reflected in ^{1}H−^{13}C WISE NMR which is suitable technique for investigation of the existence of mobility heterogeneities. It allows obtaining a combination of structural and dynamic information. Differences in molecular mobility are probed by ^{1}H line shapes, which are separated in the second dimension by the ^{13}C chemical shift. High molecular mobility results in narrowing of ^{1}H lines while rigid units produce broad signals. To obtain as selective information about segmental dynamics as possible, i.e., to avoid and suppress spin diffusion during cross-polarization, the Lee−Goldburg approach (LG-CP) was employed.

The differences in segmental mobility are quite clear in spectrum measured at 500 MHz (Figure 4A). This shows each chemically distinct ^{13}C resonance correlated with a ^{1}H powder pattern reflecting mobility. Corresponding slices through ^{1}H dimension are presented in Figure 4B. The narrow component dominates the signal of Si−CH_3 units, confirming that short siloxane chains are the most mobile part of the network. In a strictly phase-separated system substantially differing in mobility, each component is characterized by its own specific narrow or broad ^{1}H signals. If spin diffusion is permitted during the t_1 evolution and on-resonance CP, the motional narrowing proton lines can be transferred

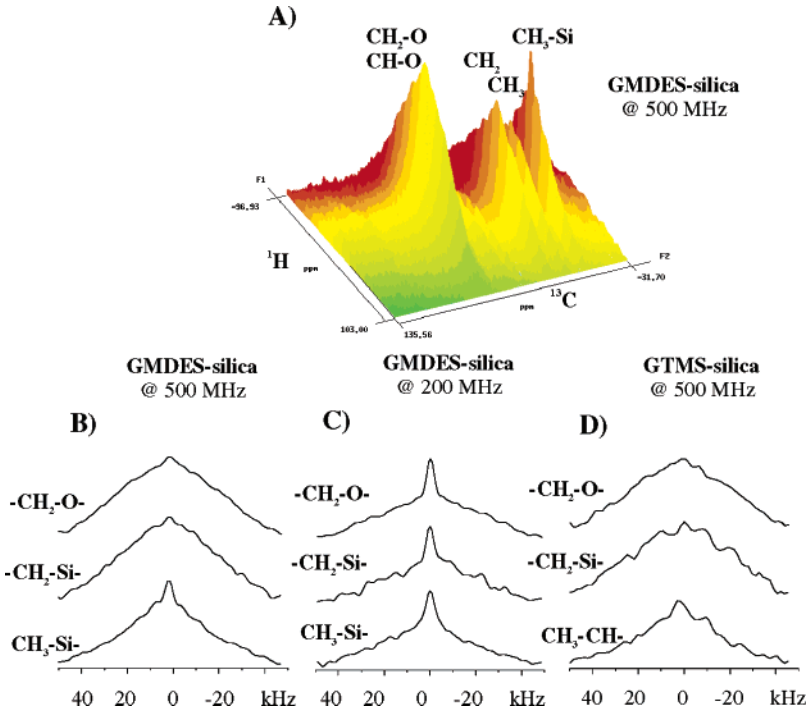

Figure 4. Stacked plot of 2D $^{1}H-^{13}C$ WISE spectra of GMDES−silica at 500 MHz (A). Selected slices through ^{1}H domain of 2D spectra of GMDES−silica system measured at 500 and 200 MHz (B and C, respectively) and GTMS−silica network measured at 500 MHz (D).

Table 2. $T_1(^{13}C)$ and $T_{1\rho}(^{13}C)$ Relaxation Times Measured at 296 K and Calculated Activation Energies of Corresponding Segmental Motions of Networks Based on GMDES (A) and GTMS (B)

	δ, ppm	group	$T_1(^{13}C)$, s	ΔE, kJ/mol	$T_{1\rho}(^{13}C)$, ms	ΔE, kJ/mol
			(A) GMDES			
GMDES silica	73.8	CH−O CH_2−O	1.7	8.7	4.7	59
	53.6	CH−N CH_2−N	4.0	7.2	6.1	73
	23.6	CH_2	0.7	8.4	3.6	48
	17.5	CH_3	0.9	6.4	9.4	39
	13.3	CH_2−Si	0.7	5.1	5.7	29
	0.1	CH_3−Si	3.5	3.0	21.1	25
GMDES	73.8	CH−O CH_2−O	2.4	6.9	4.5	35
	53.6	CH−N CH_2−N	5.7	5.0	5.2	47
	23.6	CH_2	0.7	8.4	3.2	31
	17.5	CH_3	0.7	6.0	10.5	26
	13.3	CH_2−Si	0.7	2.0	5.5	31
	0.1	CH_3−Si	3.8	1.4	28.6	26
			(B) GTMS			
GTMS silica	73.8	CH−O CH_2−O	3.1	43	3.3	45
	53.6	CH−N CH_2−N	5.8	41	3.9	47
	23.6	CH_2	1.0	23	2.9	29
	17.5	CH_3	0.9	6.4	8.9	22
	9.5	CH_2−Si	1.2	22	5.5	55
GTMS	73.8	CH−O CH_2−O	2.2	18.0	2.5	32
	53.6	CH−N CH_2−N	4.2	22.5	3.4	30
	23.6	CH_2	0.9	13.7	2.1	15
	17.5	CH_3	0.7	4.5	7.9	19
	9.5	CH_2−Si	1.0	8.2	5.0	33

to the signals of carbons of rigid segments. In intimately mixed systems these fast flip-flops (spin-diffusion) lead to equilibration of magnetization behavior. (This process is more effective at low magnetic fields (200 MHz) at which the ^{1}H NMR signal overlap is generally large, and the flip-flop interactions are not restricted.) That is why the high degree of equilibration of magnetization behavior (narrow and broad components are observed for all resolved ^{13}C signals) achieved within 1 ms of CP indicates a large degree of homogeneity and intimate mixing of oxypropylene and siloxane moieties in GMDES-based systems (Figure 4C). Segmental mobility in GTMS-based systems behaves uniformly (Figure 4D).

Ordering and Self-Organization: 2D $^{1}H-^{1}H$ CRAMPS, 2D $^{1}H-^{13}C$ HETCOR, and SAXS. To probe the extent of ordering and arrangement of various segments in these complex systems, we first performed 2D exchange experiment exploiting ^{1}H spin-diffusion with high-sensitivity ^{1}H detection using the CRAMPS technique in both time evolution domains. Application of homodecoupling sequence BR24 leads to relatively well-resolved ^{1}H spectra. The signals located on the diagonal of 2D spectra only reflects ^{1}H chemical shift of resolved structure units. (These signals provide the same information as 1D spectrum.) The off-diagonal signals correlating two different structure units subse-

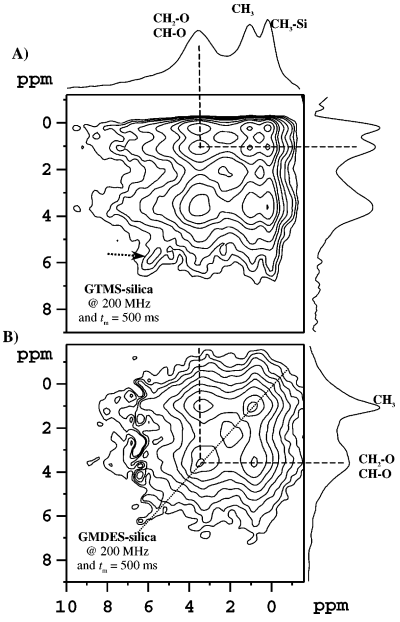

Figure 5. 2D ^{1}H−^{1}H CRAMPS spectra obtained for GTMS−silica (A) and GMDES−silica (B) networks at 200 MHz and $t_m = 500$ μs. (In upper spectrum off-diagonal signal correlating at 3.5 and 0.8 ppm is marked by dashed line. The signal of hydrogen bonded OH groups at 5.8 ppm is indicated by arrow.)

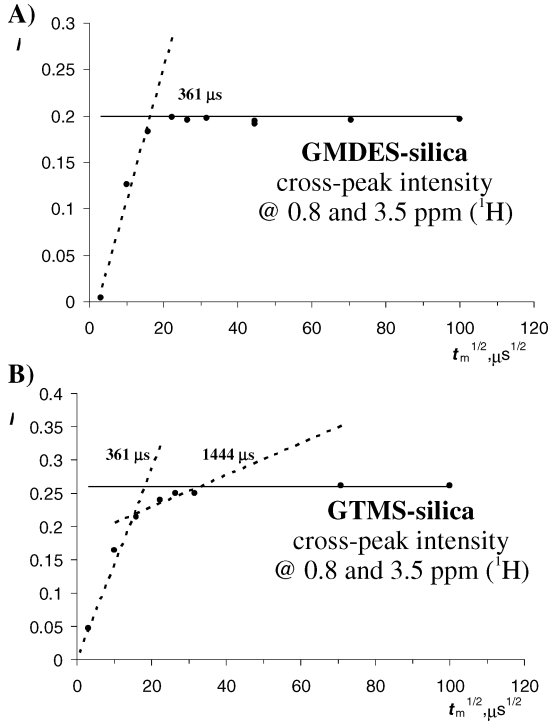

Figure 6. Spin-diffusion built-up curves of cross-peaks correlating at 0.8 and 3.5 ppm obtained for GMDES−silica (A) and GTMS−silica (B) networks.

quently indicate their spatial proximity. The dependences of off-diagonal signal intensity on spin-diffusion mixing time, t_m, correspond to ^{1}H−^{1}H interatomic distances and/or the size of domains in heterogeneous systems. Very good spectral resolution required for accurate quantitative analysis has not been achieved, however, and we were able to resolve only two or three main signals depending on chemical composition (Figure 5A,B). The off-diagonal signals correlating 3.5 and 0.8 ppm reflect mainly intramonomer magnetization exchange between CH_3 and CH−O (CH_2−O) protons.

The initial rate reflecting the intramonomer spin exchange in oxypropylene unit is the same for both spin-diffusion built-up curves, and full equilibration is achieved within $t_{eq} = 361$ μs (Figure 6A,B). For longer mixing times, during which intermonomer polarization transfer can occur, we observe a significant difference in built-up curves. In the GMDES−silica system magnetization remains constant (Figure 6A), but in the GTMS−silica system, an additional process occurs, indicating longer average distance between CH_2−Si and CH_2−O (CH−O) protons (Figure 6B). Full equilibration is achieved after $t_{eq} = 1444$ μs, reflecting segregation and ordering of oxypropylene chains and siloxane tails.

The following technique nicely combines the advantage of ^{1}H nuclei (100% isotopic abundance and high magnetogyric constant allowing observation of spin diffusion and thus providing geometrical constraints) with high resolution of ^{13}C NMR spectra. This 2D ^{1}H−^{13}C HETCOR experiment, in which ^{1}H−^{1}H spin exchange occurs during the mixing delay t_m inserted after the first ^{1}H detection period t_1, provides a significantly better resolution afforded by ^{1}H−^{13}C chemical shift separation. In the spectra we can observe in principle two types of cross-peaks. First, signals reflecting the shortest (usually one-bond) ^{1}H−^{13}C distance, and second, cross-peaks reflecting long-range through-space polarization transfer, i.e., long-range interatomic contacts. The later signals can be used to estimate geometry of the studied system. In the GTMS−silica system for a short mixing time of $t_m = 250$ μs (Figure 7A), cross-peaks for only directly bonded ^{1}H−^{13}C pairs and the shortest intra-residual contacts evolve confirming signal assignment. Even for longer $t_m = 800$ μs (Figure 7B), cross-peaks related to inter-residual transfer between oxypropylene chains and siloxane tails are very weak (marked by arrows) while contacts within and/or between the same types of monomer units still dominate. In the GMDES−silica network, short-range intra-residual contacts also dominate at mixing time $t_m = 250$ μs (Figure 8A); however, at longer time we detect a wide range of inter-residual interactions (Figure 8B). The intensities of cross-peaks (demonstrated by corresponding slices of 2D spectra) are almost equilibrated, confirming thus a much higher degree of mixing of both types of monomer units in this network compared with that based on GTMS.

Sufficient resolution of 2D ^{1}H−^{13}C HETCOR NMR spectra also allows different polarization transfer processes to be detected simultaneously and makes it possible to distinguish and determine differences in spin-diffusion coefficients for each component. This is necessary for analysis of the spin-exchange process intended for quantifying differences in organization of polymer chains in complex networks.

As we observed differences in local segmental mobility, we used the recently described[38] general strategy for direct measurement of spin diffusion within monomer units. Assuming that intrachain polarization transfer is the dominant process, spin-diffusion coefficients D were calculated from the build-up cross-peak intensity (Figure 9A,B) correlating CH_3 protons at 0.8 ppm (^{1}H) and CH_2−O (CH−O) carbons at 72 ppm (^{13}C). The initial rate of spin exchange corresponding to polarization transfer within the limited space around one oxypropylene unit is finished after $t_{eq} = 400$ and 441 μs in both systems (GTMS−silica and GMDES−silica, respectively).

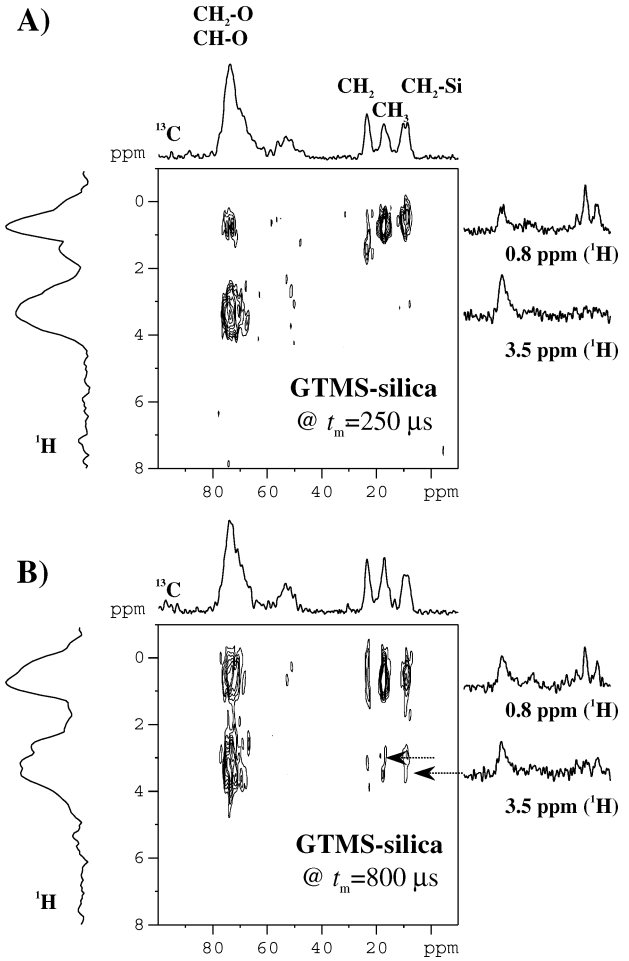

Figure 7. Comparison of 2D $^1H-^{13}C$ HETCOR (500 MHz) spectra obtained for the GTMS−silica system with spin-diffusion mixing time $t_m = 250$ (A) and 800 μs (B). Upper and left-side 1D spectra are corresponding f_2 and f_1 projections, respectively. The spectra on the right are ^{13}C slices at CH_3 (0.8 ppm) and CH_2-O (3.5 ppm) ^1H signals.

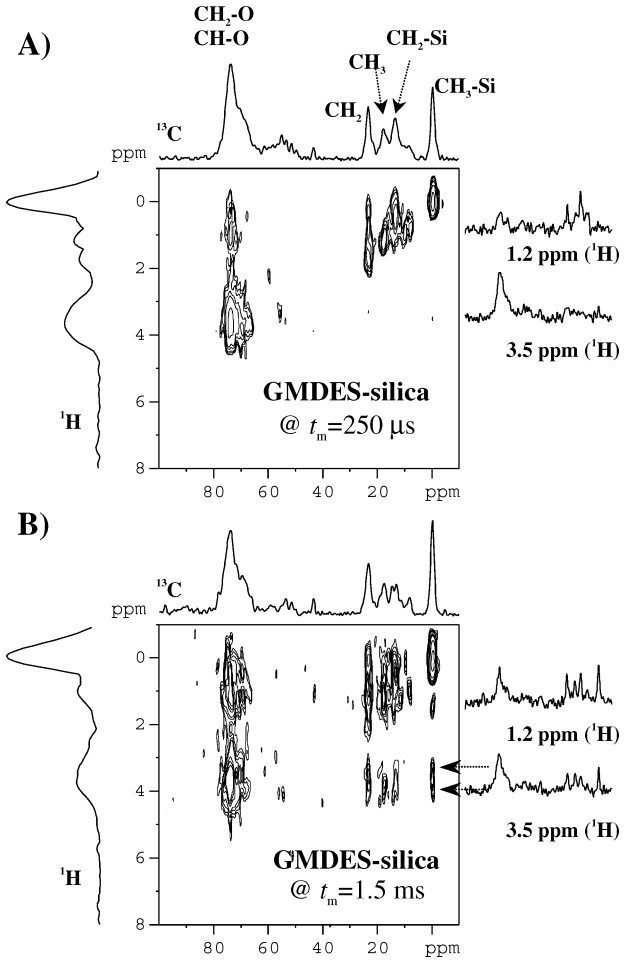

Figure 8. Comparison of 2D $^1H-^{13}C$ HETCOR spectra obtained for the GMDES−silica system with spin-diffusion mixing time $t_m = 250$ (A) and 800 μs (B). Upper and left-side 1D spectra are corresponding f_2 and f_1 projections, respectively. The spectra on the right are ^{13}C slices at CH_3 (1.2 ppm) and CH_2-O (3.5 ppm) ^1H signals.

From the known effective size of an oxypropylene unit ($x = (ld)^{1/2} = 0.35$ nm; Scheme 1), which was determined by molecular dynamic calculation as recently proposed in the literature,[38] we calculated the spin-diffusion coefficient from the following equation:[27,38]

$$D = \frac{\pi x^2}{4\epsilon^2 t_{eq}} \qquad (3)$$

where t_{eq} is the period of magnetization equilibration and ϵ is the scaling factor corresponding to dimensionality of spin-exchange process (the number of orthogonal direction along which polarization transfer from source to sink can occur). One-dimensional ($\epsilon = 1$) approximation is a suitable choice for measurement of relatively short pathways, since the protons with the shortest interatomic distances dominate polarization transfer.

The determined value of spin-diffusion coefficient $D = 0.22-0.24$ nm^2 ms^{-1} is intermediate between the values estimated for highly mobile polymers (0.05−0.15 nm^2 ms^{-1}) and rigid hard segments (0.6−0.8 nm^2 ms^{-1}). For the motionally homogeneous GTMS−silica network, the coefficient $D = 0.24-0.22$ nm^2 ms^{-1} can be used for evaluation of polarization transfer events between all segments. For the GMDES−silica network, in which CH_2-Si segments are more mobile than the rest of polymer chains, we estimated spin-exchange coefficients corresponding to these units directly by analysis of evolution of cross-peak intensity correlating CH_3-Si at 0 ppm (^1H) and $Si-CH_2$ at 10 ppm (^{13}C). From the time of equilibration $t_{eq} = 1225$ μs and the estimated average size of the structure unit ($-(O)_2Si(CH_3)-CH_2-$; $x = (ld)^{1/2} = 0.40$ nm), the calculated coefficient is equal to $D = 0.10$ nm^2 ms^{-1}, which corresponds to highly mobile polymer chains.[39] To quantify the degree of ordering and/or separation and to estimate the long pathway of polarization transfer, we analyzed the spin-exchange built-up curve (Figure 9C,D) of the cross-peak correlating the CH_2-Si carbon at 9 ppm (^{13}C) and CH_2-O (CH−O) protons at 3.5 ppm (^1H) using previously determined spin-diffusion coefficients D and eq 3. While in the GMDES−silica network, magnetization has been completely equilibrated during one step; in the GTMS−silica system, we observe a two-step process with additional increase in signal intensity due to significant portion of long-range polarization transfer reflecting separated and ordered polymer chains. The fast process reaches equilibrium within $t_{eq} = 961$ μs, reflecting a distance ca. 0.5 nm, which corresponds to polarization transfer between CH_2-Si and CH_2-O (CH−O) group within GTMS monomer unit (Scheme 2). As the full equilibration is achieved within $t_{eq} = 2209$ μs, the largest polarization transfer pathway corresponds to ca. 0.8 nm,

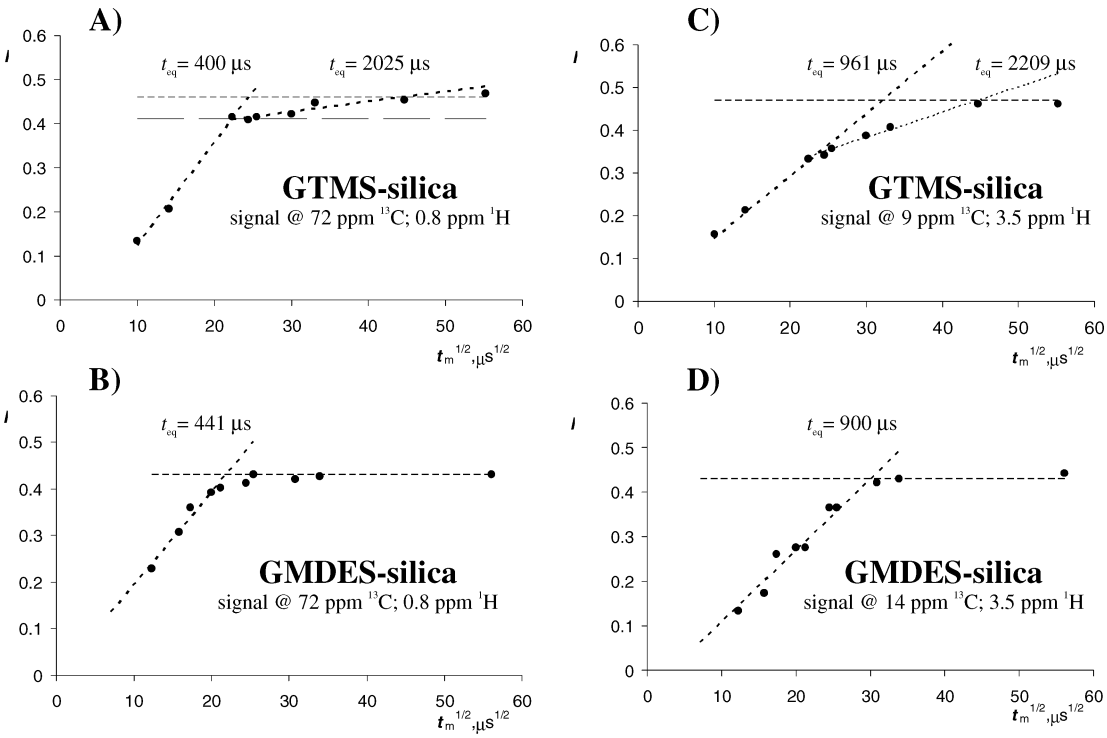

Figure 9. Spin-diffusion built-up curves of cross-peaks in ^{1}H−^{13}C HETCOR spectra correlating at 72 ppm (^{13}C) and 0.8 ppm (^{1}H) obtained for GTMS−silica (A) and GMDES−silica (B) networks and cross-peaks correlating at 9 and 3.5 ppm (C) and 14 and 3.5 ppm (D).

Scheme 2. MM+ Optimized Idealized Model of GTMS-Based Network[a]

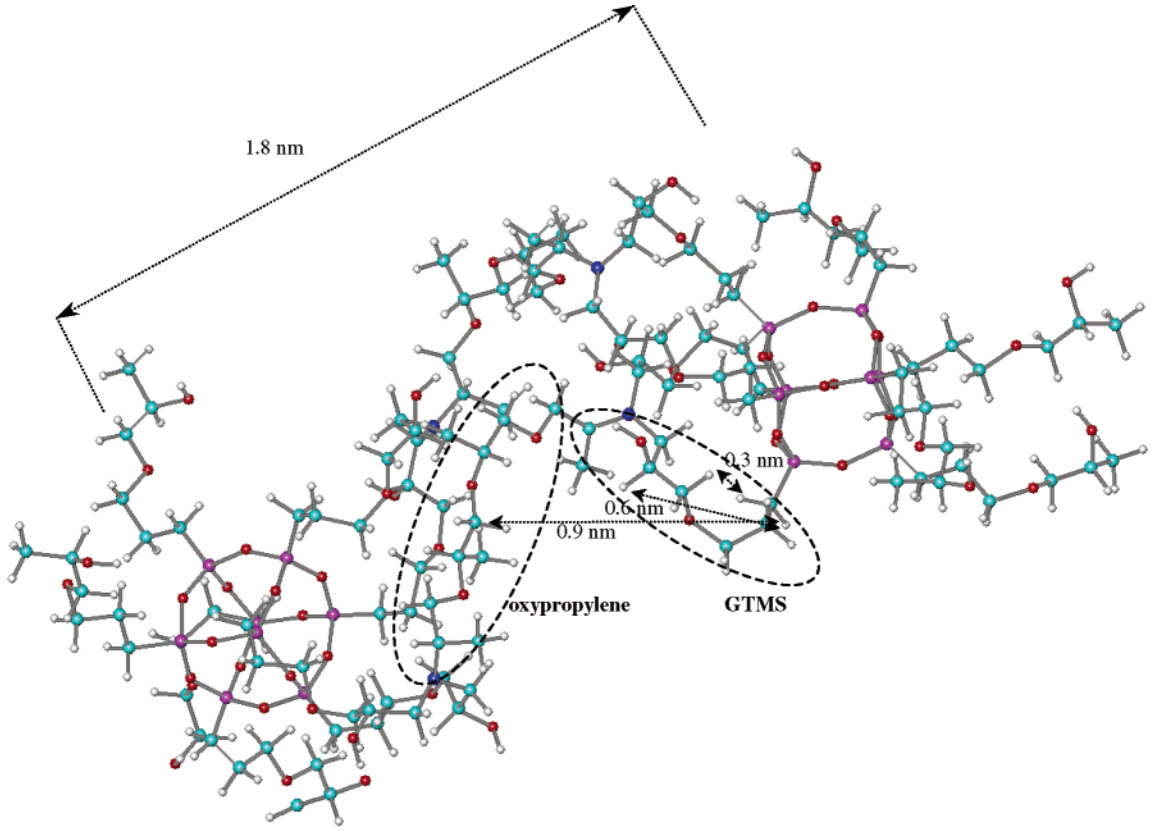

[a] Selected ^{1}H−^{1}H distances are introduced: CH_2−Si and CH_2−O (0.3 nm), CH_2−Si and CH−O (0.6 nm), and CH_2−Si and CH_2−O (0.9 nm).

which roughly reflects the largest distance between CH_2−O (CH−O) in oxypropylene units and CH_2−Si protons on the surface of siloxane clusters. (In the network, the largest distance corresponds to the middle of the CH_2O− chain.) This finding indicates significant spatial separation of GTMS residues and oxypropylene chains, which are concentrated between siloxane cage-like clusters. In contrast, in the GMDES−silica network,

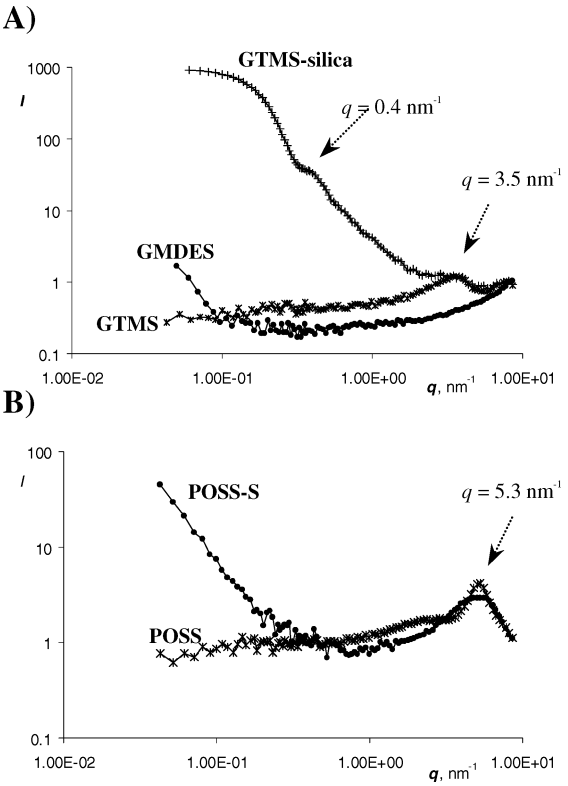

Figure 10. Comparison of SAXS scattering curves obtained for system containing in situ prepared siloxane cagelike clusters (GTMS, GTMS−silica, and GMDES; A) and for neat POSS particles and for network prepared by block polymerization with D230 (POSS-S; B).

magnetization is rapidly equilibrated during $t_{eq} = 900$ μs. As segmental dynamics in this network is significantly variable, we used the average value of $D_{eff} = (0.22 + 0.10)/2 = 0.16$ nm^2 ms^{-1} to evaluate the spin-diffusion process between oxypropylene units and CH_2−Si protons. The resulting value confirms that GMDES−silica systems (neglecting presence of silica particles) are in fact homogeneous, and individual segments of various monomer units are mixed within the 0.45 nm region.

The presence of silica in prepared networks has no significant influence on the long-range order of all studied systems as confirmed by SAXS. The high scattering intensity at low scattering vector $q \rightarrow 0$ reflects a random distribution of silica particles in the polymer matrix. A small hump at $q = 0.4$ nm^{-1} reflects the size of silica particles which is ca. 29 nm. While GMDES-based products do not show any regular arrangement, the GTMS-based analogues exhibit a high degree of regularity and ordering within the whole volume. The long-range ordered "two-phase" structure is clearly detected through the interference maximum at the scattering vector $q = 3.5$ nm^{-1} reflecting correlation distances of $\xi = 1.79$ nm (Figure 10A), which can be interpreted as the average distance between siloxane cagelike clusters. The oxypropylene chains form well-organized phase-separating organic tails of siloxane clusters, thus providing links between epoxy-functionalized cagelike units.

The low scattering intensity at $q \rightarrow 0$ confirms the long-range order of all siloxane cagelike clusters in the network and their uniform size. The observed value $\xi = 1.79$ nm well corresponds to the spin-diffusion-determined value of ca. 0.8 nm, which reflects the distance between the center of oxypropylene phase and the surface of siloxane cluster (Scheme 2).

A high degree of long-range order of GTMS-based networks is further confirmed by comparison of these scattering curves with those of the systems prepared from regular POSS building blocks at very similar and predominantly comparable reaction conditions. Neat POSS forms physical network where siloxane cages are regularly distributed and separated by their organic tails (Figure 10B). The corresponding average distance between cages is $\xi = 1.18$ nm. Because of the polymerization of these POSS units with functionalized oxypropylene chains in block or solution (POSS-B, POSS-S), the interference maxima are slightly shifted and broadened, corresponding to $\xi = 1.36$ or 1.26 nm, respectively. Smaller values of these distances, compared with the correlation distance observed for GTMS-based systems, reflect that in situ formed cagelike clusters are larger containing more than eight silicon atoms. In both cases we observe a significant scattering intensity at low vectors ($q \rightarrow 0$), reflecting the diffraction from individual cages randomly distributed in oxypropylene chains. This corresponds to a low conversion of oxirane groups (ca. 30%) during block polymerization (POSS-B) and to fast evaporation of the solvent (propan-2-ol) during thermal curing (80 °C; POSS-S). The escape of the solvent (under conditions comparable with preparation of GTMS-based systems) is too fast for cages to regularly organize. (GTMS-based systems are prepared from a solution containing a large amount of water while water-insoluble POSS materials are polymerized from propan-2-ol only.) The evaporation of a water-containing solution is much slower, which makes partial reorganization of individual cagelike clusters possible.

Silica Polymer Interaction: 2D ^{1}H−^{29}Si HETCOR. Although SAXS did not indicate any influence of silica particles on the long-range order of all studied systems, some chemical or physical interaction between silica surface and polymer matrix was detected by the ^{1}H−^{29}Si HETCOR experiment. Well-pronounced correlation signals between polymer matrix and silica particles indicating their specific interaction were clearly detected for the GTMS−silica system only (Figure 11A). Correlation between CH_2−Si protons and Q^4 silicon atoms indicates mutual chemical binding. In the GMDES−silica network, no correlation between silica and CH_2−Si or CH_3−Si was detected (Figure 11B), indicating thus no specific interaction between polymers and silica particles. This fact probably results from a significantly higher segmental mobility of its short siloxane chains, thus preventing formation of mutual bonding with silica.

Atomic Force Microscopy. AFM was used for a high-resolution study of surface morphology. The measurements in the tapping and contact modes were evaluated to test the possibility of the surface destruction and to compare surface images. If the normal force of the tip did not exceed tens of nanonewtons, no destruction of the surface was detected in the contact mode, and the same information on the surface morphology was obtained as in the tapping mode. If normal forces of the probe on the sample were high enough (of the order of 10^2 nN) and were repeatedly applied to the surface, the formation of scrapes of different shape and depth was observed depending on the value of the normal force and the number of applications (Figure 12). Hence, we performed quantitative determination of the

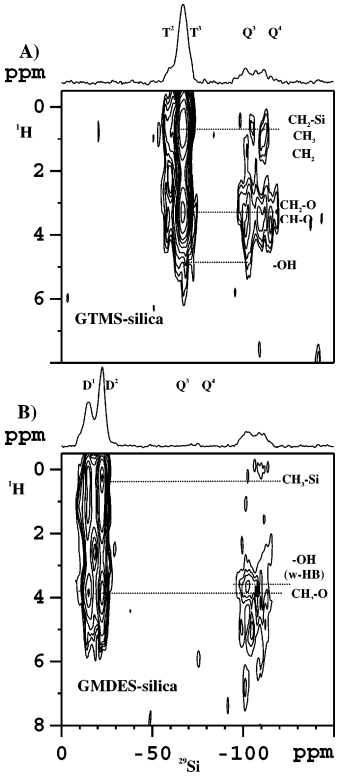

Figure 11. Comparison of 2D $^{1}H-^{29}Si$ HETCOR spectra obtained for GTMS−silica (A) and GMDES−silica networks (B) with spin-diffusion mixing time $t_m = 5$ ms. Possible correlations between structure units are indicated by dashed lines.

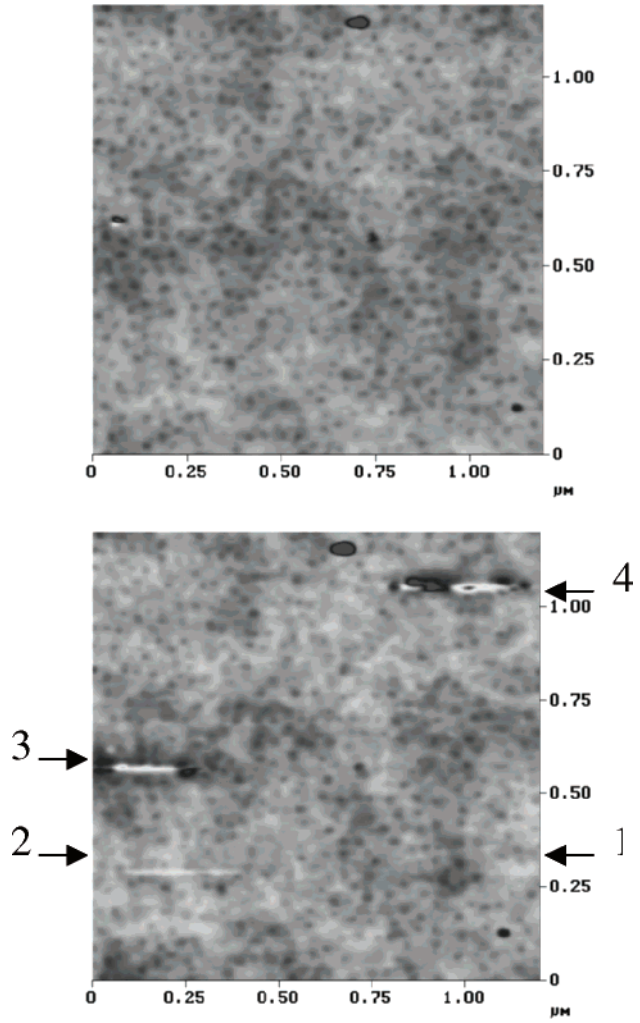

Figure 12. Surface image of GTMS−silica network before (top) and after destruction (bottom) by the OTR-8PS probe. The normal force, F_n, applied for 30 s on the length 350 nm: 100 nN (1), 170 nN (2), 240 nN (3), and 370 nN (4); velocity: 4 μm s^{-1}. Normal force used for imaging: 25 nN.

scratch resistance. In contrast to reported homemade diamond tips[40−43] having a spring constant of the 10^2 N/m order, we used a commercial silicon nitride tip with the spring constant 0.68 N/m, commonly used for nondestructive surface imaging. The resulting scratch resistances[43] S_r are listed in Table 1. The highest scratch resistance shows the ductile GMDES−silica network, while the lowest S_r was found for harder silica-free GTMS one. Our observation is in accord with the general finding that the scratch resistance of coatings is enhanced by increasing ductility (elasticity) of products and in the presence of inorganic nanoparticles.[42−46] The destruction of surfaces in $x-y$ coordinates confirmed that these nanocomposite films are characterized by different local stiffness/elasticity on the nanometer scale. All hybrid films have fairly flat (units of nanometers) and regular surfaces; the surface smoothness and profile depend on the presence/absence of colloidal SiO_2 particles. The presence of individual SiO_2 nanoparticles well incorporated into the surface layer is well observed (Figure 12). Their distribution on the surface is uniform, without distinct clustering. It was estimated that SiO_2 nanoparticles, which are well miscible with all reactants and fairly compatible with the formed O−I networks, tend to partially concentrate at the surface layer lowering thus the surface tension. A similar concentration of small silica particles on the coating surface was observed in polyester and melamine resin,[44] while in the acrylic-based polyurethane systems the concentration of silica micro- and nanoparticles on the surface was not observed.[4] Although the prepared networks differ substantially in tensile properties, they exibit similar values of scratch resistance, reflecting that surface properties are influenced by the mechanical properties of the matrix to a limited extent and can be varied and controlled by the presence and concentration of nanoadditives.

Conclusion

As hybrid organic−inorganic networks vary substantially in final properties, detailed studies of the reaction mechanism and investigation of structure, arrangement, and dynamics at segmental level are necessary to understand the nature of processes leading to the targeted macroscopic properties of these complex systems.

It was demonstrated by solid-state NMR spectroscopy, SAXS, and AFM that highly self-organized and long-range ordered epoxide-based networks are formed under certain conditions from functionalized siloxane building blocks (GTMS), functionalized oligo(oxypropylene)diamine, and colloidal silica nanoparticles. Time-dependent NMR experiments lead to optimization of reaction conditions, which allow to separate the sol−gel and polyaddition steps and thus to control the whole process. This is a necessary prerequisite for the design and manufacture of functional materials. We have found that the duration of “alkaline” step (in which various inorganic precondensates arise) and the presence of

colloidal silica (accelerating polycondensation) have a dominant influence on final properties of the resulting films. NMR study revealed that highly condensed (q_i = 0.85) isolated polycyclic cagelike clusters must be formed before their aggregation during the sol−gel steps. Subsequently, during thermal curing of these starlike epoxy-functionalized building blocks, all oxirane rings are consumed. The presence of silica nanoparticles promotes cyclization of siloxanes and thus formation of highly condensed and rigid cagelike clusters in the GTMS system, while only short oligomers with a significant fraction of cycles are formed in the GMDES one. The differences in the structure of the inorganic phase are reflected in segmental mobility as probed by NMR relaxation experiments and, consequently, result in various elasticity of final products. The GMDES-based system manifests enhanced elasticity due to flexible CH_2−Si segments in contrast to GTMS-based analogues in which these segments are immobilized in cagelike clusters. 2D $^1H-^1H$ CRAMPS and $^1H-^{13}C$ HETCOR NMR and SAXS experiments confirmed that GMDES-based systems are homogeneous without any regular long-range arrangement, while GTMS-based systems exhibit high degrees of regularity and self-ordering throughout the bulk. The cagelike clusters with uniform size are regularly dispersed within the polymer matrix. Their average distance is ca. 1.7 nm, and oxypropylene chains form a well-organized phase which separates organic tails of siloxane clusters and also provides links between epoxy-functionalized cagelike units. The determined distance between the center of the oxypropylene phase and the siloxane cluster surface is 0.8 nm. Although silica particles do not affect the long-range order of the studied systems, specific interaction between the silica surface and polymer matrix in the GTMS−silica network was detected through the $^1H-^{29}Si$ HETCOR experiment. Slow segmental mobility of siloxane units built in in cagelike clusters does not prevent chemical and physical bonding with the surface of silica nanoparticles. These particles are partially concentrated on the surface of prepared films and thus increase scratch resistance as determined by AFM.

Acknowledgment. The authors thank the Grant Agency of the Czech Republic (203/01/0735) and the Grant Agency of Academy of Sciences the Czech Republic (A 4050008 and KSK 4050111) for financial support.

References and Notes

(1) Lange, J.; Luisier, A.; Hult, A. *J. Coat. Technol.* **1997**, *69*, 77.
(2) Yaneff, P. V.; Adamsons, K.; Ryntz, R. A.; Britz, D. *J. Coat. Technol.* **2002**, *74*, 135.
(3) Xiang, C.; Sue, H. J.; Chu, J.; Coleman, B. *J. Polym. Sci., Polym. Phys.* **2001**, *39*, 47.
(4) Zhou, S. X.; Wu, L. M.; Sun, J.; Shen, W. D. *Prog. Org. Coat.* **2002**, *45*, 33.
(5) Brinker, C. J.; Scherer, C. W. In *Sol−Gel Science*; Academic Press: San Diego, 1990.
(6) Matejka, L.; Dukh, O.; Brus, J.; Simonsick, W. J.; Meissner, B. *J. Non-Cryst. Solids* **2000**, *270*, 34.
(7) Kickelbick, G. *Prog. Polym. Sci.* **2003**, *28*, 83.
(8) Davis, S. R.; Brough, A. R.; Atkinson, A. *J. Non-Cryst. Solids* **2003**, *315*, 197.
(9) Daniels, M. W.; Francis, L. F. *J. Colloid Interface Sci.* **1998**, *205*, 191.
(10) Daniels, M. W.; Sefcik, J.; Francis, L. F.; Cormick, A. V. M. *J. Colloid Interface Sci.* **1999**, *219*, 351.
(11) Bauer, F.; Sauerland, V.; Gläsel, H.-J.; Ernst, H.; Findeisen, M.; Hartmann, E.; Langguth, H.; Marqardt, B.; Mehnert, R. *Macromol. Mater. Eng.* **2002**, *287*, 546.
(12) Bauer, F.; Sauerland, V.; Ernst, H.; Glasel, H. A.; Naumov, S.; Mehnert, R. *Macromol. Chem. Phys.* **2003**, *204*, 375.
(13) Pouxviel, J. C.; Boilot, J. P.; Beloeil, J. C.; Lallemand, J. Y. *J. Non-Cryst. Solids* **1987**, *89*, 345.
(14) Brus, J.; Dybal, J. *Polymer* **1999**, *40*, 6933.
(15) Špírková, M.; Brus, J.; Hlavatá, D.; Kamišová, H.; Matějka, L.; Strachota, A. *J. Appl. Polym. Sci.*, accepted for publication.
(16) Špírková, M.; Brus, J.; Hlavatá, D.; Kamišová, H.; Matějka, L.; Strachota, A. *Surf. Coat. Int.* **2003**, *86*, *B3*, 187.
(17) Wen, J.; Vasudevan, V. J.; Wilkes, G. L. *J. Sol-Gel Sci. Technol.* **1995**, *5*, 115.
(18) Kasemann, R.; Schmidt, H. *New J. Chem.* **1994**, *18*, 1117.
(19) Ni, H.; Johnson, A. H.; Soucek, M. D.; Grant, J. T.; Vreugdenhil, A. J. *Macromol. Mater. Eng.* **2002**, *287*, 470.
(20) Hou, S. S.; Bonagamba, T. J.; Beyer, F. L.; Madison, P. H.; Schmidt-Rohr, K. *Macromolecules* **2003**, *36*, 2769.
(21) Ying, D. K.; Zax, D. B. *J. Phys. Chem.* **1999**, *110*, 5325.
(22) Hou, S. S.; Beyer, F. L.; Schmidt-Rohr, K. *Solid State Nucl. Magn. Reson.* **2002**, *22*, 110.
(23) De Paul, S. M.; Zwanziger, J. W.; Ulrich, R.; Wiesner, U.; Spiess, H. W. *J. Am. Chem. Soc.* **1999**, *121*, 5736.
(24) Pawsey, S.; McCormick, M.; De Paul, S.; Graf, R.; Lee, Y. S.; Reven, L.; Spiess, H. W. *J. Am. Chem. Soc.* **2003**, *125*, 4174.
(25) Brown, S. P.; Spiess, H. W. *Chem. Rev.* **2001**, *101*, 4125.
(26) Wu, X.; Burns, T.; Zilm, K. W. *J. Magn. Reson. A* **1994**, *111*, 29.
(27) Schmidt-Rohr, K.; Clauss, J.; Spiess, H. W. *Macromolecules* **1992**, *25*, 3273.
(28) Lee, M.; Goldburg, W. I. *Phys. Rev. A* **1965**, *140*, 1261.
(29) van Rossum, B. J.; de Groot, C. P.; Ladizhansky, V.; Vega, S.; de Groot, H. J. M. *J. Am. Chem. Soc.* **2000**, *122*, 3465.
(30) van Rossum, B. J.; Schulten, E. A. M.; Raap, J.; Oschkinat, H.; de Groot, H. J. M. *J. Magn. Reson.* **2002**, *155*, 1.
(31) Bennet, A. E.; Rienstra, C. M.; Auger, M.; Lakshmi, K. V.; Griffin, R. G. *J. Chem. Phys.* **1995**, *103*, 6951.
(32) Burum, D. P.; Rhim, W. K. *J. Chem. Phys.* **1979**, *71*, 944.
(33) Caravatti, P.; Neuenschwander, P.; Ernst, R. R. *Macromolecules* **1985**, *18*, 119.
(34) Chernenko, S. P.; Cheremukhina, G. A.; Fateev, O. V.; Smykov, L. P.; Vasiliev, S. E.; Zanevsky, Yu. V.; Kheiker, D. M.; Popov, A. N. *Nucl. Instrum. Methods Phys. Res., Ser. A* **1994**, *348*, 261.
(35) Devreux, F.; Boilot, J. P.; Chaput, F.; Lecomte, A. *Phys. Rev. A* **1990**, *41*, 6901.
(36) Brunner, E.; Sternberg, U. *Prog. Nucl. Magn. Reson. Spectrosc.* **1998**, *32*, 21.
(37) Robert, E.; Whittington, A.; Fayon, F.; Pichavant, M.; Massiot, D. *Chem. Geol.* **2001**, *174*, 291.
(38) Jia, X.; Wolak, J.; Wang, X.; White, J. L. *Macromolecules* **2003**, *36*, 712.
(39) Brus, J.; Dybal, J.; Sysel, P.; Hobzová, R. *Macromolecules* **2002**, *35*, 1253.
(40) Bai, M. W.; Kato, K.; Umehara, N.; Miyake, Y.; Xu, J. G.; Tokisue, H. *Surf. Coat. Technol.* **2000**, *126*, 181.
(41) Shen, W. D.; Juany, B.; Gasworth, S. M.; Mukamal, H. *Tribol. Int.* **2001**, *34*, 135.
(42) Jones, F. N.; Shen, W.; Smith, S. M.; Huna, Z.; Ryntz, R. A. *Prog. Org. Coat.* **1998**, *34*, 119.
(43) Shen, W.; Ji, C.; Jones, F.; Everson, M. P.; Ryntz, A. *Surf. Coat. Int.* **1997**, *79*, 253.
(44) Frings, S.; van Nostrum, C. F.; van der Linde, R.; Meinema, H. A.; Rentrop, C. H. A. *J. Coat. Technol.* **2000**, *74*, 83.
(45) Zhou, S. X.; Wu, L. M.; Sun, J.; Shen, W. D. *Prog. Org. Coat.* **2002**, *45*, 33.
(46) Wang, D. K.; Moon, J. H.; Shul, Y. G.; Jung, K. T.; Kim, D. H.; Lee, D. *J. Sol-Gel Sci. Technol.* **2003**, *26*, 783.

MA035608H